EES Catalysis

PAPER

View Article Online
View Journal



Cite this: DOI: 10.1039/d6ey00017g

# A conjugated coordination polymer enables efficient proton supply on the platinum surface for alkaline hydrogen evolution electrocatalysis

Shuting Zhan,[a] Yunxia Liu,[b] Xinyue Xu,[a] Yan Liu,[c] Ziwei Ma,[a] Shouhan Zhang,[a] Li Hu,[a] Haiping Lin,[d] Longsheng Zhang *[a] and Tianxi Liu[a]

Developing a high-performance alkaline hydrogen evolution reaction (HER) catalyst is of great significance for scalable hydrogen production from water electrolysis. However, the alkaline HER kinetics are impeded by sluggish water dissociation and inefficient proton supply required for its proton-coupled electron transfer process. Herein, we report a facile and effective method to prepare a high-performance alkaline HER catalyst consisting of platinum (Pt) nanoparticles immobilized onto a conductive conjugated coordination polymer (CCP) that is enriched with homogeneous and flexibly regulated single-atom metal sites (15–20 wt%), which can effectively promote water dissociation to ensure efficient proton supply for the active Pt nanoparticles. For a proof-of-concept study, three catalysts consisting of Pt nanoparticles immobilized onto three analogous CCPs with single-atom nickel, copper and cobalt sites were comparatively investigated. The alkaline HER activities of these three catalysts surprisingly follow the same order as the abilities of the single-atom metal sites of CCPs for water dissociation. Our *in situ* electrochemical impedance spectroscopy, carbon monoxide stripping and kinetic isotope measurements, combined with theoretical studies, unambiguously verify the essential role of the single-atom metal sites of CCP support materials in facilitating alkaline HER kinetics. This strategy opens an alternative avenue for promoting various catalytic reactions that necessitate proton supply from water dissociation.

Received 23rd January 2026,
Accepted 14th April 2026

DOI: 10.1039/d6ey00017g

rsc.li/eescatalysis



## Broader context

Developing efficient and stable catalysts for the alkaline hydrogen evolution reaction (HER) is a pivotal step towards large-scale green hydrogen production *via* water electrolysis. Among all other catalysts, platinum (Pt)-based catalysts are some of the most appropriate HER catalysts due to their favorable adsorption energies of HER intermediates, which unfortunately suffer from sluggish water dissociation and an inefficient proton supply rate in alkaline media, thereby leading to unsatisfactory alkaline HER kinetics. In this study, we report a general and effective strategy to develop a novel alkaline HER catalyst with Pt nanoparticles immobilized onto conjugated coordination polymers with densely integrated and flexibly tunable single-atom sites to accelerate water dissociation for efficient proton supply to the adjacent Pt nanoparticles. Our study, comparing nickel, copper and cobalt single-atom-based conjugated coordination polymers establishes a clear correlation between the alkaline HER activity and the intrinsic water-dissociation capability of their single-atom sites. This strategy of constructing a functional support-active nanoparticle catalytic system transcends the specific reaction, offering a versatile avenue towards enhancing widespread catalytic systems that involve proton-coupled electron transfer processes.

## 1. Introduction

Hydrogen is of great importance to clean energy systems due to its renewable nature, environmental compatibility and high energy density.[1–5] Notably, water electrolysis is a sustainable and efficient approach to convert electrical energy into hydrogen, where the oxygen evolution reaction and the hydrogen evolution reaction (HER) are the anodic and cathodic reactions.[6–10] Among the developed HER catalysts, platinum (Pt) stands out as the most effective catalyst for the HER

[a] *Key Laboratory of Synthetic and Biological Colloids, Ministry of Education, School of Chemical and Material Engineering, Jiangnan University, Wuxi 214122, China. E-mail: zhangls@jiangnan.edu.cn*
[b] *School of Chemistry and Chemical Engineering, Northwestern Polytechnical University, Xi'an 710072, China*
[c] *Department of Chemistry, National University of Singapore, Singapore 117543, Singapore*
[d] *School of Physics and Information Technology, Shaanxi Normal University, Xi'an 710062, China*

because of its near-optimal free energy for hydrogen adsorption, delivering the highest HER activity.[11–13] However, Pt catalysts exhibit HER activities in alkaline media that are 2–3 orders of magnitude slower compared to those in acidic media.[14,15]

The HER under alkaline conditions takes place with the adsorption of water molecules onto the catalyst surface, followed by the dissociation of water to generate adsorbed hydrogen intermediates (*H) and finally the generation and evolution of $H_2$.[16,17] It requires an initial water dissociation step (Volmer step: $H_2O + e^- \rightarrow *H + OH^-$) to generate *H, followed by hydrogen transfer steps (Heyrovsky: $*H + H_2O + e^- \rightarrow H_2 + OH^-$ and Tafel: $2*H \rightarrow H_2$).[18–20] However, the additional energy barrier of water dissociation and the inefficient proton supply rate mitigate the performance improvement of alkaline HER catalysts.[21–26] Facilitating the alkaline HER necessitates improving both water dissociation kinetics and the proton supply rate, with an emphasis on accelerating the water dissociation kinetics.[27,28]

Here, we report a general and effective strategy to develop a novel alkaline HER catalyst consisting of Pt nanoparticles supported on conjugated coordination polymers (CCPs). Notably, the CCP materials feature high-density, uniformly distributed and elaborately tunable single-atom metal sites (15–20 wt%) with highly adjustable coordination environments, which arise from the diverse organic ligands and metal precursors employed in their synthesis.[29–34] As an emerging class of support materials, CCPs hold immense potential toward developing advanced composite catalysts targeted for various catalytic reactions. Benefiting from their unique attributes, the CCP materials are expected to effectively facilitate water dissociation and enhance alkaline HER kinetics. For a comparative study, three composite catalysts consisting of Pt nanoparticles supported on three analogous CCPs enriched with single-atom nickel (Ni), copper (Cu) and cobalt (Co) sites were synthesized (Fig. 1a). For simplicity, the resulting composite catalysts are denoted as Pt/Ni-CCP, Pt/Cu-CCP and Pt/Co-CCP, respectively. Our electrochemical measurement results indicate that Pt/Ni-CCP exhibits appreciably higher alkaline HER performance relative to Pt/Cu-CCP and Pt/Co-CCP. Furthermore, both the experimental results and the theoretical calculations revealed that the abilities of the single-atom Ni, Cu and Co sites of CCP support materials for water dissociation follow the same order as the alkaline HER activities of these three composite catalysts. Compared to the single-atom Cu and Co sites, the single-atom Ni sites exhibit a higher ability for water dissociation, leading to

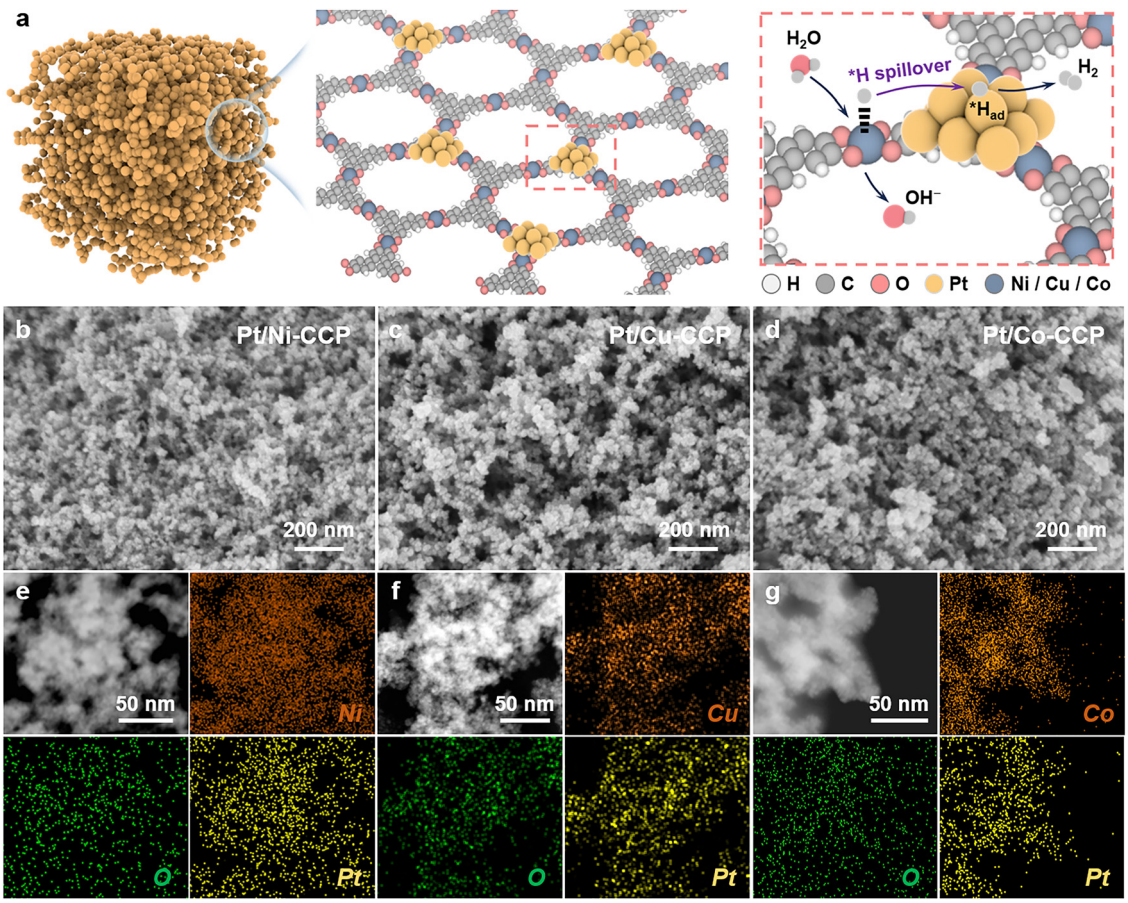


Fig. 1 (a) Schematic illustration of the structure of the Pt/M-CCP (M = Ni, Cu, and Co) catalyst consisting of Pt nanoparticles supported on a conjugated coordination polymer and its advantage in accelerating $H_2O$ dissociation, *H spillover and $H_2$ production during the alkaline HER process. (b)–(d) SEM images of Pt/Ni-CCP, Pt/Cu-CCP and Pt/Co-CCP, respectively. (e)–(g) Element mapping images of Pt/Ni-CCP, Pt/Cu-CCP and Pt/Co-CCP, respectively.

greatly enhanced alkaline HER kinetics of Pt/Ni-CCP. These results strongly validate the essential role of the single-atom metal sites of CCP support materials in promoting water dissociation and ensuring efficient proton supply on the surface of active Pt sites. This strategy holds immense potential for the design of high-performance catalysts for widespread catalytic reactions that necessitate efficient proton supply from water dissociation.

# 2. Experimental

## 2.1. Chemicals

Sodium borohydride ($NaBH_4$), nickel acetate tetrahydrate ($Ni(OAc)_2{\cdot}4H_2O$), copper acetate monohydrate ($Cu(OAc)_2{\cdot}H_2O$), cobalt acetate tetrahydrate ($Co(OAc)_2{\cdot}4H_2O$), dimethyl sulfoxide (DMSO), ethanol, and potassium hydroxide (KOH) were purchased from Sinopharm Chemical Reagent Co. Ltd. Potassium tetrachloroplatinate ($K_2PtCl_4$) was brought from Shanghai Aladdin Biochemical Technology Co. Ltd. 2,3,6,7,10,11-Hexahydroxytriphenyl (HHTP) was brought from InnoChem Technology Co., Ltd. Carbon paper (HCP-030N) was purchased from Toray Industries Co., Ltd. Nafion dispersion (5 wt%) and Pt/C catalyst (20 wt%) were brought from Sigma-Aldrich. $IrO_2$ catalyst was brought from the Shanghai Adamas Reagent Co., Ltd. Deuterium water was purchased from Energy Chemical Co., Ltd.

## 2.2. Synthesis of Pt/Ni-CCP, Pt/Cu-CCP, and Pt/Co-CCP

Ni-CCP was synthesized as follows: 130 mg of HHTP and 199 mg of $Ni(OAc)_2{\cdot}4H_2O$ were dispersed into 10 mL of a mixed solution of deionized water and DMSO (v/v, 1 : 1) under ultrasonication for 30 min in a vial. Subsequently, the vial was sealed and heated at 85 °C for 24 h. The resultant black precipitate was collected *via* centrifugation and vacuum drying. Similarly, Cu-CCP was prepared using 68.3 mg of $Cu(OAc)_2{\cdot}H_2O$ and 75 mg of HHTP, while Co-CCP was prepared using 92 mg of $Co(OAc)_2{\cdot}4H_2O$ and 60 mg of HHTP. Afterward, the Pt/Ni-CCP, Pt/Cu-CCP and Pt/Co-CCP catalysts were prepared through the $NaBH_4$ reduction method by employing Ni-CCP, Cu-CCP and Co-CCP as the support materials. Taking Pt/Ni-CCP as an example, in a typical synthesis, Ni-CCP (50 mg) and $K_2PtCl_4$ (12 mg) were dispersed into deionized water (20 mL) in a vial by using ultrasonic treatment. Subsequently, the contents of the vials were stirred for another 6 h to ensure sufficient adsorption. Then, $NaBH_4$ (945 mg) was dispersed into deionized water (20 mL) in a vial and added to the above dispersion. Finally, the resultant black precipitate was collected through centrifugation and vacuum drying. Accordingly, Pt/Cu-CCP and Pt/Co-CCP were synthesized through the same procedure by replacing Ni-CCP with Cu-CCP and Co-CCP, respectively.

## 2.3. Electrochemical measurements

Electrochemical tests were conducted using an Autolab M204 workstation. Carbon rod and Hg/HgO (filled with 1 M KOH solution) were employed as the counter and reference electrodes, respectively. Prior to the electrochemical measurements, the Hg/HgO reference electrode was calibrated against a reversible hydrogen electrode (RHE). A continuous flow of $H_2$ gas into a 1 M KOH aqueous electrolyte was maintained for 60 min before and during the calibration experiment. Based on the obtained cyclic voltammetry curves, the potential of zero current is −0.091 V for the Hg/HgO reference electrode. All potentials were converted to reversible hydrogen electrode (RHE) using the equation: $E_{RHE} = E_{(Hg/HgO)} + 0.091 + 0.059 \times pH$. The working electrodes were prepared as follows: the catalyst suspension was first prepared by mixing 5 mg of the catalyst, 80 μL of CNT dispersion, 500 μL of ethanol, and 80 μL of Nafion dispersion, followed by ultrasonication for 60 min to form a homogeneous ink. Then, 10 μL of the suspension was drop-cast onto each side of a carbon paper substrate (0.5 cm × 0.5 cm), resulting in a total catalyst loading of approximately 0.15 mg $cm^{-2}$. The working electrode was dried at room temperature overnight before testing. The linear sweep voltammetry (LSV) tests at a scan rate of 5 mV $s^{-1}$ were carried out in Ar-saturated 1 M KOH aqueous solution. All experiments were carried out 25 ± 1 °C and repeated at least three times to ensure reproducibility.

## 2.4. *In situ* EIS and CO-stripping experiments

The *in situ* EIS and CO-stripping experiments were both carried out in a typical three-electrode configuration similar to that used for HER performance evaluation. Pt foil and Hg/HgO (filled with 1 M KOH solution) were employed as the counter and reference electrodes, respectively. The *in situ* EIS experiment was conducted in an Ar-saturated 1 M KOH aqueous solution, with the frequency set from $1 \times 10^5$ to $1 \times 10^{-2}$ at an amplitude of 0.01 V. The CO-stripping experiment was carried out in a CO-saturated 1 M KOH aqueous solution, where CO gas was purged through the solution for 30 mins to allow CO molecules to be adsorbed onto the catalyst surface. Then, a chronoamperometric activation step was performed at a constant potential of −0.1 V (*vs.* RHE) for 30 mins. Finally, cyclic voltammetry was carried out with a potential range of 0–1.2 V (*vs.* RHE) at a scan rate of 20 mV $s^{-1}$.

# 3. Results and discussion

## 3.1. Synthesis and characterization of catalysts

First, we prepared the Pt/Ni-CCP, Pt/Cu-CCP, and Pt/Co-CCP catalysts through a facile method (see details in the Experimental section). As observed in the scanning electron microscopy (SEM) characterization (Fig. 1b–d), Pt/Ni-CCP, Pt/Cu-CCP and Pt/Co-CCP all exhibit granular morphologies with porous structures. The energy dispersive spectroscopy (EDS) mapping results demonstrate that the Ni/Cu/Co, O and Pt elements are uniformly distributed within Pt/Ni-CCP, Pt/Cu-CCP, and Pt/Co-CCP (Fig. 1e–g and Fig. S1, SI), respectively. Additionally, the transmission electron microscopy (TEM) characterization studies reveal that the loaded Pt nanoparticles in these three catalysts exhibit uniform size distribution ranging from 2 to 5 nm and the high-resolution TEM images display distinct

lattice fringes with a spacing of ~0.22 nm for Pt/Ni-CCP, Pt/Cu-CCP, and Pt/Co-CCP, which can be ascribed to the (111) plane of metallic Pt (Fig. S2–S4, SI).[35–37] The inductively coupled plasma–mass spectrometry measurements reveal that the Pt weight percentages in Pt/Ni-CCP, Pt/Cu-CCP and Pt/Co-CCP are 31.0, 31.6 and 29.8 wt%, respectively. The X-ray diffraction (XRD) results validate the existence of Pt metals in Pt/Ni-CCP, Pt/Cu-CCP and Pt/Co-CCP samples (Fig. 2a). Subsequently, X-ray photoelectron spectroscopy (XPS) was used to detect Pt nanoparticles (Fig. S5–S7, SI). The coordination status and bonding configurations of Pt in the catalysts were probed by X-ray absorption spectroscopy at the Pt $L_3$-edge. Fig. 2b and Fig. S8 (SI) display the X-ray absorption near edge structure (XANES) and extended X-ray absorption fine structure (EXAFS) spectra which indicate that Pt/Ni-CCP, Pt/Cu-CCP, and Pt/Co-CCP exhibit similar characteristics with Pt–Pt interactions within the Pt nanoparticles and Pt–C interactions derived from the metal–support interactions between Pt atoms and C atoms. As depicted in Fig. 2c, the coordination environments in Pt/Ni-CCP, Pt/Cu-CCP and Pt/Co-CCP can be further revealed by the intensity maxima in their wavelet-transformed EXAFS (WT-EXAFS) results. The results of Ni XANES of Pt/Ni-CCP, Ni foil, NiO, and NiPc, and EXAFS of Pt/Ni-CCP, Ni foil, NiO, and NiPc at the *k* space are presented in Fig. S9 (SI). Notably, the EXAFS spectrum of Pt/Ni-CCP is different from those of Ni foil, NiO and NiPc, which unambiguously verifies the single-atom Ni features of Pt/Ni-CCP. Fig. 2d depicts the EXAFS spectra of Pt/Ni-CCP, Ni foil, NiO, and NiPc; the three catalyst samples show a prominent peak, markedly different from Ni foil with a notable metallic peak. No metallic peak of Ni was found in

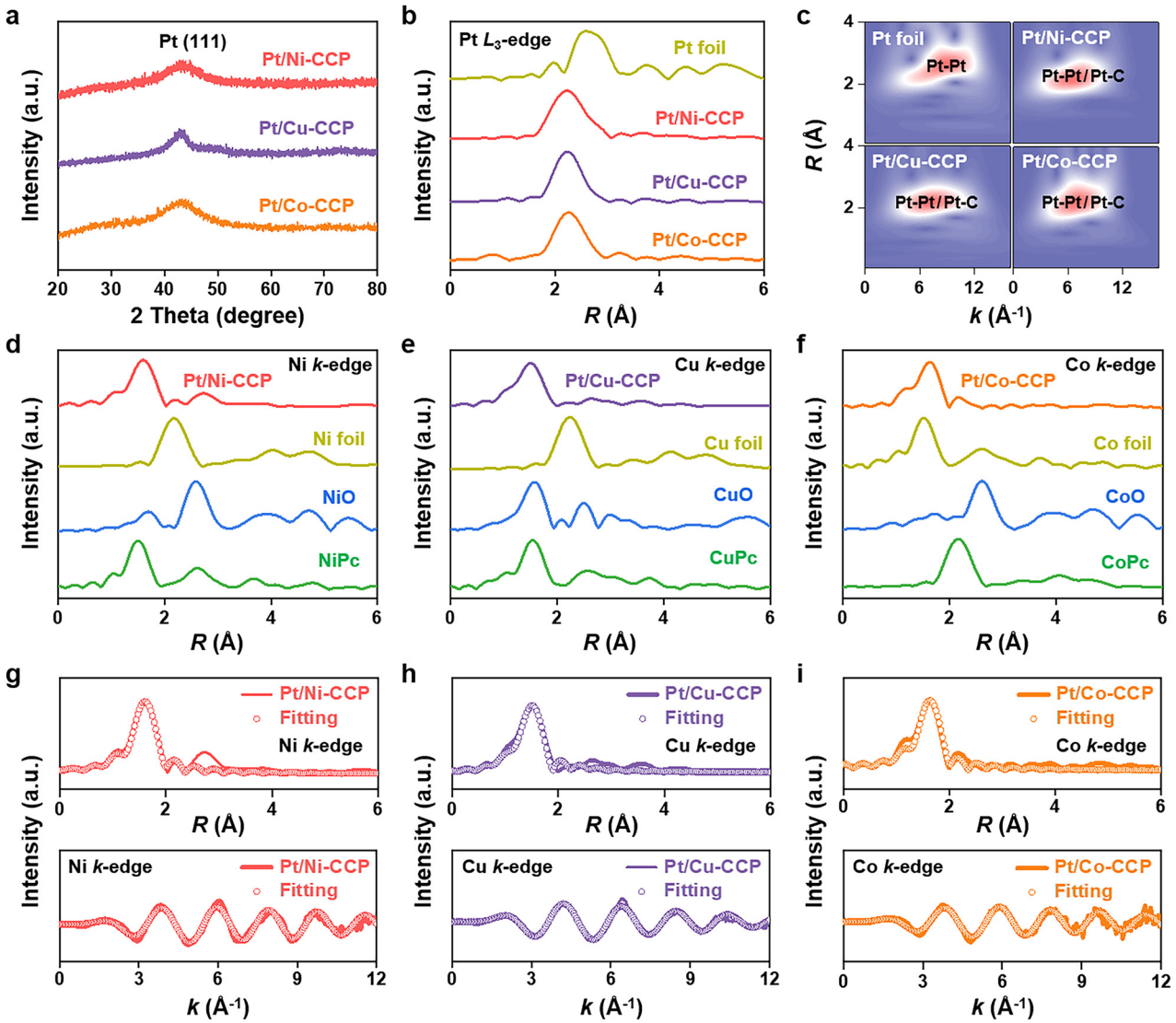


Fig. 2 (a) XRD patterns of Pt/Ni-CCP, Pt/Cu-CCP and Pt/Co-CCP. (b) and (c) Pt $L_3$-edge EXAFS spectra and Wavelet-transform analysis of Pt foil, Pt/Ni-CCP, Pt/Cu-CCP and Pt/Co-CCP. (d) Ni k-edge EXAFS spectra of Pt/Ni-CCP, Ni foil, NiO and NiPc. (e) Cu k-edge EXAFS spectra of Pt/Cu-CCP, Cu foil, CuO and CuPc. (f) Co k-edge EXAFS spectra of Pt/Co-CCP, Co foil, CoO and CoPc. (g)–(i) Fitted EXAFS curves of Pt/Ni-CCP, Pt/Cu-CCP, and Pt/Co-CCP at *R* and *k* spaces, respectively.

the EXAFS spectra of Pt/Ni-CCP, thus excluding the existence of a metallic Ni component in this catalyst sample. The EXAFS fitting results of Pt/Ni-CCP are presented in Fig. 2g, which reveal the local coordination structures of $NiO_4$ with bonding distances of ~2.04 Å. Moreover, as exhibited in Fig. S10 (SI), we conducted WT-EXAFS for Pt/Ni-CCP, Ni foil, NiO and NiPc. Comparison of their wavelet transform plots can also verify the Ni-single-atom features in Pt/Ni-CCP with intensity maximum (~4.9 $Å^{-1}$, ~1.5 Å), in sharp contrast to those of Ni foil (~7.2 $Å^{-1}$, ~2.2 Å), NiO (~6.8 $Å^{-1}$, ~2.6 Å) and NiPc (~5.5 $Å^{-1}$, ~1.4 Å). Similarly, Pt/Cu-CCP and Pt/Co-CCP exhibit characteristic single-atom features for Cu and Co, validated by XANES, EXAFS, and WT-EXAFS (Fig. 2e, f, h, i, and Fig. S11–S14, SI).

### 3.2. Performance evaluation

The alkaline HER electrocatalytic activities of Pt/Ni-CCP, Pt/Cu-CCP, Pt/Co-CCP and commercial Pt/C (20 wt%) catalysts were measured in 1 M KOH aqueous solution. All potentials *versus* the Hg/HgO reference electrode were calibrated to the reversible hydrogen electrode (RHE) scale (Fig. S15, SI). Fig. 3a and Fig. S16–S20 (SI) present that Pt/Ni-CCP achieves a current density of 10 mA $cm^{-2}$ at an overpotential of only 36.7 mV, markedly lower than those of Pt/Cu-CCP (81.2 mV), Pt/Co-CCP (146.8 mV) and commercial Pt/C (48.0 mV). As displayed in Table S1 (SI), the Pt/Ni-CCP catalyst demonstrates a lower overpotential than most reported alkaline HER catalysts. Concurrently, LSV analysis of the pristine M-CCP (M = Ni, Cu, and Co) catalysts without any Pt nanoparticles exhibits low HER activity (Fig. S21, SI), thereby highlighting the indispensable role of Pt nanoparticles in HER catalytic performance. In addition, we evaluated the mass activities (MA) and specific activities (SA) of Pt/Ni-CCP, Pt/Cu-CCP, and Pt/Co-CCP by referencing the measured currents to their electrochemically active surface area. At −0.1 V (*vs.* RHE), Pt/Ni-CCP exhibits a high MA of 1255.6 mA $mg_{Pt}^{-1}$, surpassing Pt/Cu-CCP (366.4 mA $mg_{Pt}^{-1}$) and Pt/Co-CCP

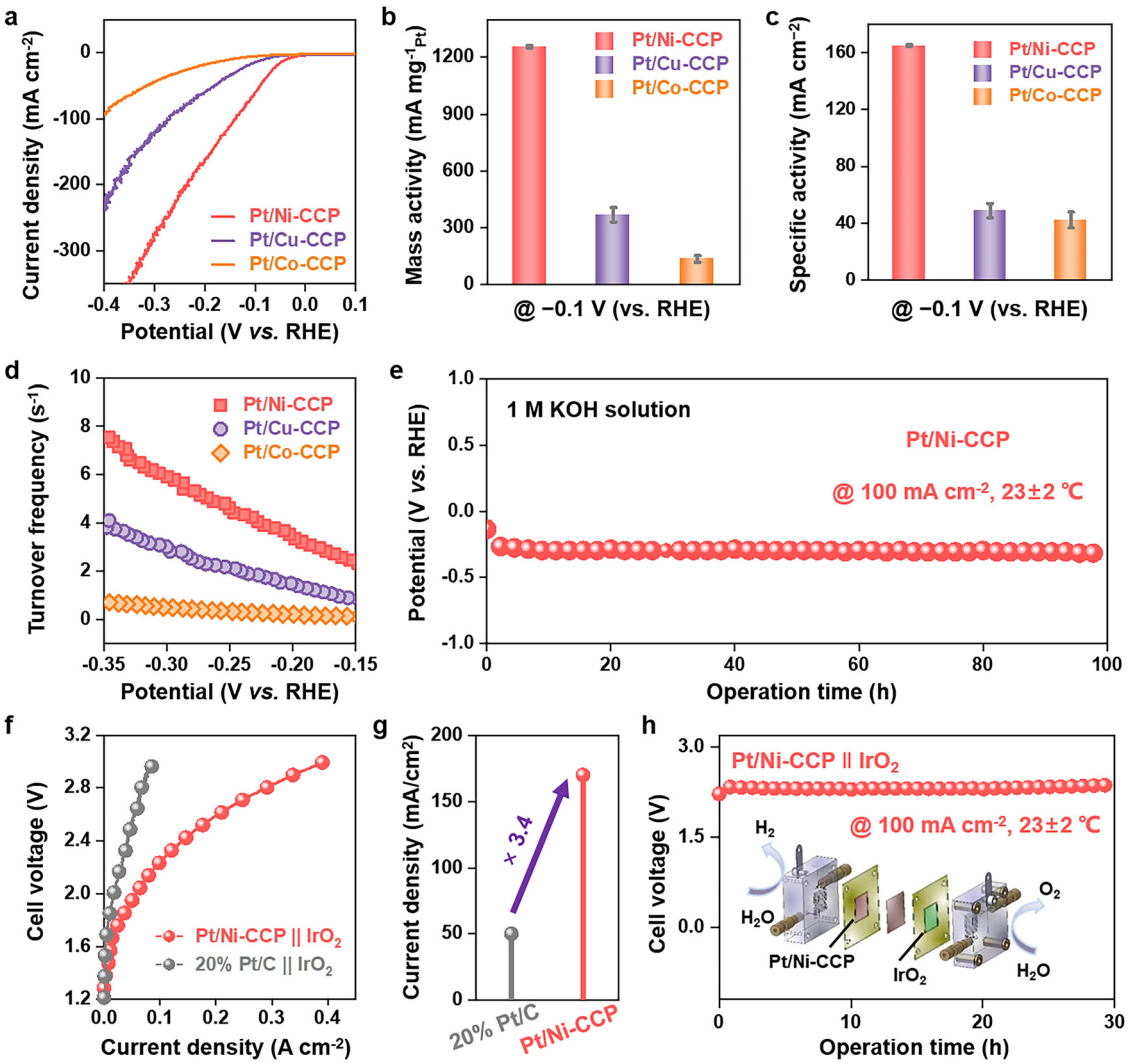


Fig. 3 (a) LSV curves of Pt/Ni-CCP, Pt/Cu-CCP and Pt/Co-CCP. (b)–(d) Comparison of the MA, SA and TOF of Pt/Ni-CCP, Pt/Cu-CCP and Pt/Co-CCP, respectively. (e) Galvanostatic test of Pt/Ni-CCP operated at 100 mA $cm^{-2}$. (f) LSV curves of Pt/Ni-CCP ‖ $IrO_2$ and Pt/C ‖ $IrO_2$ cells for water electrolysis. (g) Current densities of Pt/Ni-CCP ‖ $IrO_2$ and Pt/C ‖ $IrO_2$ cells at 2.5 V. (h) Galvanostatic test of the Pt/Ni-CCP ‖ $IrO_2$ cell operated at 100 mA $cm^{-2}$.

(133.2 mA $mg_{Pt}^{-1}$) (Fig. 3b). Moreover, as demonstrated in Fig. 3c and Fig. S22–S24 (SI), Pt/Ni-CCP exhibits a high SA of 165.0 mA $cm^{-2}$ at −0.1 V (*vs.* RHE), exceeding those of Pt/Cu-CCP (48.8 mA $cm^{-2}$) and Pt/Co-CCP (42.1 mA $cm^{-2}$). Moreover, we also calculated the turnover frequency (TOF) of Pt/Ni-CCP, Pt/Cu-CCP and Pt/Co-CCP (Fig. 3d), in which Pt/Ni-CCP was found to markedly surpass Pt/Cu-CCP and Pt/Co-CCP, suggesting its superior intrinsic HER activity. By normalizing the currents to the specific surface area values from the Brunauer–Emmett–Teller (BET) measurements (Fig. S25, SI), the specific activity of Pt/Ni-CCP was found to be 1811.0 mA $m_{BET}^{-2}$ at −0.1 V (*vs.* RHE), surpassing those of Pt/Cu-CCP (451.5 mA $m_{BET}^{-2}$) and Pt/Co-CCP (102.1 mA $m_{BET}^{-2}$). As presented in Fig. 3e, we performed the galvanostatic measurements for Pt/Ni-CCP at 100 mA $cm^{-2}$ for a continuous operation of 100 h, in which negligible decay was observed, suggesting its good stability. Furthermore, the post-mortem XRD and XPS analyses (Fig. S26, SI) of Pt/Ni-CCP suggested that the structures and valence states of Pt nanoparticles show no discernible variations before and after the acidic HER electrocatalysis, revealing its robust structural integrity. To evaluate the practical applicability of the Pt/Ni-CCP catalyst, we assembled an alkaline water electrolyzer using Pt/Ni-CCP (cathode) and $IrO_2$ (anode). Fig. 3f displays the LSV curves of the alkaline water electrolyzer with Pt/Ni-CCP and Pt/C catalyst cathodes. Remarkably, at a cell voltage of 2.5 V, the current density of the alkaline water electrolyzer with Pt/Ni-CCP surpasses that of the Pt/C by a factor of 3.4 (Fig. 3g). Moreover, the alkaline water electrolyzer with Pt/Ni-CCP shows exceptional operational stability (Fig. 3h), maintaining a steady performance for 30 h operated at 100 mA $cm^{-2}$. Collectively, these results demonstrate that Pt/Ni-CCP displays excellent HER activity, demonstrating its huge potential as a superior electrocatalyst for alkaline water electrolysis.

### 3.3. Theoretical calculation and mechanism investigation

Fig. 4a presents the proposed alkaline HER mechanism on Pt/M-CCP catalysts with accelerated $H_2O$ dissociation, *H spillover and $H_2$ production. The energy barrier for cleaving the OH–H bond in water ($\Delta G_{H_2O}$) is 0.11 eV on Pt/Ni-CCP, which is significantly lower than those on the Pt/Cu-CCP (0.28 eV) and Pt/Co-CCP (0.61 eV) (Fig. 4b). This indicates that the Ni sites could greatly accelerate the sluggish water dissociation. As shown in Fig. S27 (SI), compared to the single-atom Cu and Co in Pt/Cu-CCP and Pt/Co-CCP, the single-atom Ni in Pt/Ni-CCP features a markedly higher d-band center, indicating its stronger water dissociation ability that leads to enhanced alkaline HER performance of Pt/Ni-CCP. The thermodynamic advantage of the Volmer step directly correlates with the enhanced interfacial hydroxyl adsorption capability, as probed by CO-stripping measurements. CO-stripping measurements were employed to assess the hydroxyl ($OH^-$) adsorption capability of the catalysts, as the CO oxidation process is intrinsically associated with the availability of $OH^-$ reactants on the catalyst surface.[38,39] Cyclic voltammetry curves recorded in CO-saturated 1 M KOH (Fig. 4c) reveal distinct CO-oxidation peaks for Pt/Ni-CCP, Pt/Cu-CCP, and Pt/Co-CCP at 0.51, 0.55, and 0.60 V (*vs.* RHE), respectively. The significantly lowered

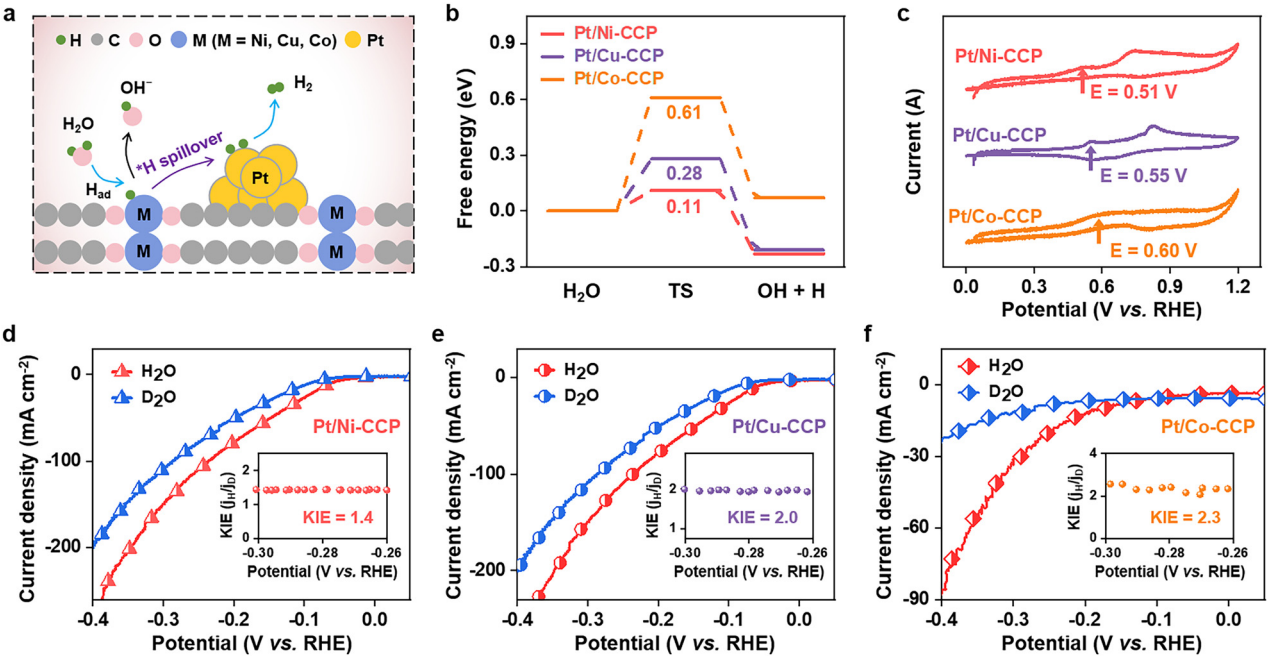


Fig. 4 (a) Schematic illustration of the proposed alkaline HER mechanism on the Pt/M-CCP (M = Ni, Cu, and Co) catalyst with accelerated $H_2O$ dissociation, *H spillover and $H_2$ production. (b) Free energy diagram of the Pt/Ni-CCP, Pt/Cu-CCP and Pt/Co-CCP models toward alkaline HER electrocatalysis. (c) Cyclic voltammetry curves of Pt/Ni-CCP, Pt/Cu-CCP and Pt/Co-CCP from the CO-stripping measurements. (d)–(f) LSV curves of Pt/Ni-CCP, Pt/Cu-CCP and Pt/Co-CCP from KIE experiments. Insets in (d)–(f) are the corresponding KIE values that are defined as the ratio of current densities obtained with $H_2O$ and $D_2O$ as solvents.

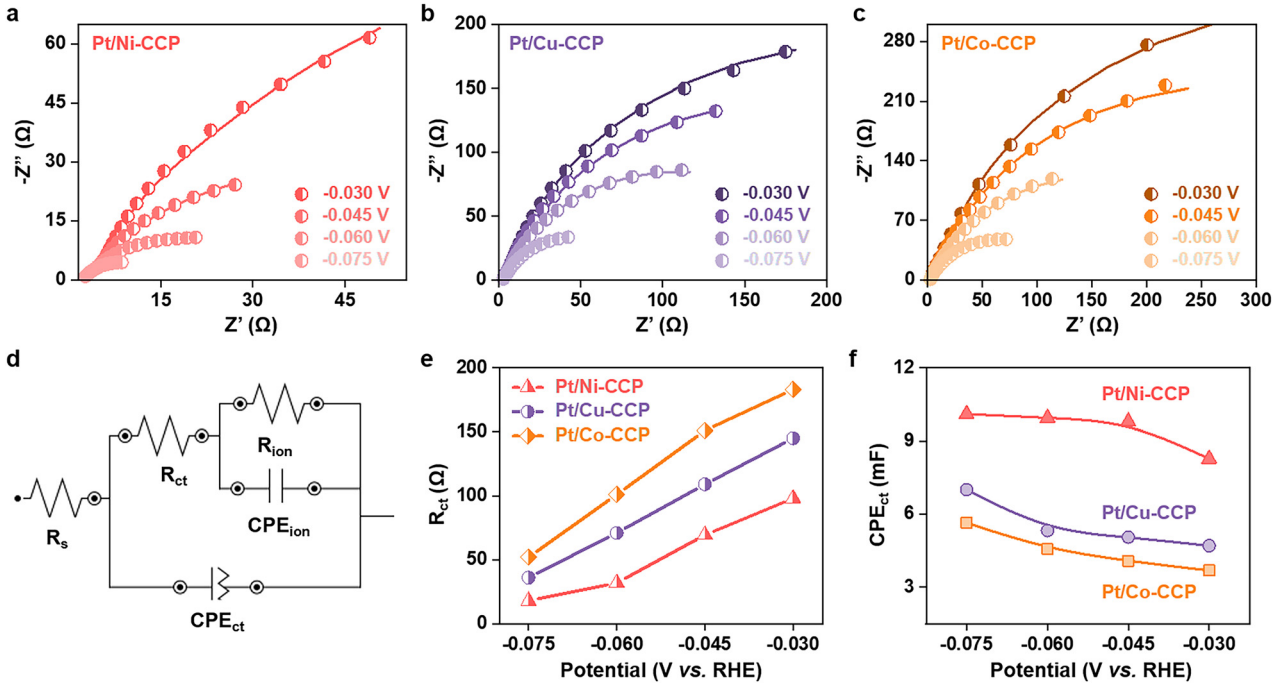


Fig. 5 (a)–(c) Nyquist plots from the *in situ* EIS measurements for Pt/Ni-CCP, Pt/Cu-CCP and Pt/Co-CCP at different applied potentials, respectively. (d) Equivalent circuit diagram for the *in situ* EIS measurement. (e) and (f) Comparing the $R_{ct}$ and $CPE_{ct}$ values as a function of applied potentials for Pt/Ni-CCP, Pt/Cu-CCP and Pt/Co-CCP, respectively.

oxidation potential of Pt/Ni-CCP compared to that of Pt/Cu-CCP and Pt/Co-CCP indicates its superior capability to stabilize adsorbed $OH^-$ intermediates, which could promote the structural percolation of hydrogen-bonding networks, thereby facilitating proton-coupled electron transfer kinetics in the alkaline HER. Moreover, the measurement of kinetic isotope effect (KIE) assists in determining whether the rate-determining step involves the transfer of protons. In an alkaline medium, water dissociation is the main source of protons, and the energy barrier toward cleaving the O–D bond is higher than that of O–H. The lower value of kinetic isotope effect (KIE) (Fig. 4d–f) indicates faster hydrogen transfer kinetics.[40–42] It can be seen that the KIE value of Pt/Ni-CCP is 1.4, which is significantly lower than those of Pt/Cu-CCP (2.0) and Pt/Co-CCP (2.3). The smaller KIE value of Pt/Ni-CCP implies superior hydrogen formation and transfer kinetics. To elucidate the mechanism of alkaline HER kinetics, *in situ* electrochemical impedance spectroscopy (EIS) for Pt/Ni-CCP, Pt/Cu-CCP, and Pt/Co-CCP was further carried out at different applied potentials, which can operando track the reaction intermediates at the catalyst surface.[43] In the Nyquist plots (Fig. 5a–c), Pt/Ni-CCP displayed greatly smaller semicircular arcs than its counterparts, indicative of lower charge-transfer resistance.[44] We further used an equivalent circuit to fit the Nyquist curves and obtained the solution resistance ($R_s$), charge transfer resistance and capacitance ($R_{ct}$ and $CPE_{ct}$), and ion adsorption resistance and capacitance ($R_{ion}$ and $CPE_{ion}$).[45–47] As seen in Fig. 5e, Pt/Ni-CCP exhibits a lower $R_{ct}$ in the alkaline HER, where *H desorption acts as the rate-determining step of charge transfer. The decreased $R_{ct}$ values of Pt/Ni-CCP indicate its accelerated *H desorption kinetics, while the elevated $CPE_{ct}$ values (Fig. 5f) suggest a higher density of accessible active sites. The above observations evidence a high coverage of *H intermediates on the catalyst surface, contributing to the superior alkaline HER activity of Pt/Ni-CCP as observed.

## 4. Conclusion

In summary, we demonstrate a novel design of an efficient alkaline HER electrocatalyst consisting of Pt nanoparticles supported onto conjugated coordination polymers enriched with well-defined single-atom metal sites that can facilitate water dissociation to provide efficient proton supply for effectively improving the alkaline HER kinetics on the Pt sites. For a proof-of-concept study, three analogous electrocatalysts consisting of Pt nanoparticles supported onto Ni-CCP, Cu-CCP and Co-CCP were investigated. The electrochemical measurements indicate that Pt/Ni-CCP displays markedly enhanced mass activity and specific activity compared to Pt/Cu-CCP and Pt/Co-CCP. Furthermore, the detailed experimental and theoretical studies suggest that, relative to the single-atom Cu and Ni sites, the single-atom Ni sites of the CCP support material can significantly lower the thermodynamic barrier of the water dissociation step and enable efficient proton supply for alkaline HER electrocatalysis on the Pt sites. Overall, this strategy not only facilitates water dissociation towards efficient alkaline HER catalysis, but also provides valuable insights for developing high-performance catalysts targeted for widespread catalytic reactions that necessitate proton supply from water dissociation. The exploration of CCP as the supporting material

for advanced composite catalysts beyond the HER remains an underexplored challenge that warrants dedicated future effort.

## Conflicts of interest

The authors declare no conflict of interest.

## Data availability

The data that support the findings of this study are available in the supplementary information (SI) of this article. Supplementary information including the results from TEM, SEM, XPS, XANES, EXAFS, LSV, and BET analysis. See DOI: https://doi.org/10.1039/d6ey00017g.

## Acknowledgements

S. Zhan and Y. Liu contributed equally to this work. This work was supported by the National Natural Science Foundation of China (52373211) and the Fundamental Research Funds for the Central Universities (2232019A3-03). This work was carried out with the support of the BL14W1 beamline at the Shanghai Synchrotron Radiation Facility.

## References

1 L. Hou, Z. Li, H. Jang, M. Kim, J. Cho, W. Zhong, S. Liu and X. Liu, *Angew. Chem., Int. Ed.*, 2025, **64**, e202423756.
2 L. Zhang, J. Bai, S. Zhang, Y. Liu, J. Ye, W. Fan, E. Debroye and T. Liu, *ACS Nano*, 2024, **18**, 22095.
3 R. Ram, L. Xia, H. Benzidi, A. Guha, V. Golovanova, A. Garzón Manjón, D. Llorens Rauret, P. Sanz Berman, M. Dimitropoulos, B. Mundet, E. Pastor, V. Celorrio, C. Mesa, A. Das, A. Pinilla-Sánchez, S. Giménez, J. Arbiol, N. López and F. García de Arquer, *Science*, 2024, **384**, 1373–1380.
4 J. Bai, Y. Liu, Z. Ma, S. Zhang, G. Chao, H. Lin, E. Debroye, L. Zhang and T. Liu, *Sci. China: Chem.*, 2024, **67**, 2063–2069.
5 Z. Seh, J. Kibsgaard, C. Dickens, I. Chorkendorff, J. Nørskov and T. Jaramillo, *Science*, 2017, **355**, eaad4998.
6 L. Zhang, H. Yuan, L. Wang, H. Zhang, Y. Zang, Y. Tian, Y. Wen, F. Ni, H. Song, H. Wang, B. Zhang and H. Peng, *Sci. China Mater.*, 2020, **63**, 2509–2516.
7 L. Zhang, S. Zhang, J. Bai, Y. Ding, J. Ye, Y. Song, E. Debroye, W. Fan and T. Liu, *Chem. Commun.*, 2024, **60**, 6821–6824.
8 H. Shen, Y. Huang, P. Zhao, R. Gao, Z. Wei, X. Gao, M. Liao, W. Dai, X. Liu, D. Sui, J. Liu, S. Zhu and Y. Wei, *Adv. Funct. Mater.*, 2026, **36**, e14862.
9 M. Deshmukh, A. Bakandritsos and R. Zbořil, *Nano-Micro Lett.*, 2025, **17**, 1.
10 Z. Zhi, X. Fan, X. Tian, J. Niu, T. Sun, D. Li, L. Zhang and D. Yang, *Compos. Commun.*, 2025, **57**, 102452.
11 Z. Wu, J. Bai, F. Lai, H. Zheng, Y. Zhang, N. Zhang, C. Wang, Z. Wang, L. Zhang and T. Liu, *Sci. China Mater.*, 2023, **66**, 2680–2688.
12 S. Zhang, Z. Wu, Y. Liu, J. Bai, Y. Ding, Z. Ma, H. Lin, L. Zhang and T. Liu, *Adv. Energy Mater.*, 2025, **15**, 2403945.
13 Q. Yang, J. Zeng, G. Yang, X. Sun, X. Lin, K. Liu, J. Chen, S. Wang and X. F. Lu, *EES Catal.*, 2025, **3**, 972–993.
14 G. Shi, T. Tano, D. Tryk, A. Iiyama, M. Uchida, K. Terao, H. Osada, M. Yamaguchi, K. Tamoto and K. Kakinuma, *ACS Catal.*, 2024, **14**, 9460–9468.
15 C. Ma, W. Chen, Y. Wu, W. Wang, L. Xu, C. Chen, L. Zheng, G. Wang, P. Han, P. Gu, X. Wang, Y. Zhu, Z. Zeng, H. He, Q. He, Z. Ke, D. Su and Y. Chen, *Nano Lett.*, 2025, **25**, 3212–3220.
16 X. Xiao, Z. Li, Y. Xiong and Y. Yang, *J. Am. Chem. Soc.*, 2023, **145**, 16548–16556.
17 Q. Qin, H. Jang, X. Jiang, L. Wang, X. Wang, M. Kim, S. Liu, X. Liu and J. Cho, *Angew. Chem., Int. Ed.*, 2024, **63**, e202317622.
18 F. Sun, Q. Tang and D. Jiang, *ACS Catal.*, 2022, **12**, 8404–8433.
19 S. Wen, L. Yan and X. Zhao, *Adv. Energy Mater.*, 2025, **15**, 2502432.
20 L. Xiao, C. Cheng, T. Yang, J. Zhang, Y. Han, C. Han, W. Lv, H. Tan, X. Zhao, P. Yin, C. Dong, H. Liu, X. Du and J. Yang, *Adv. Mater.*, 2024, **36**, 2411134.
21 W. Chen, C. Xu, H. Yu, H. Huang, S. Li, Y. Cao, W. Peng, Y. Li, H. Ke, S. Xu, H. Mo, C. Wu, H. Wang, Y. Zhang and X. Li, *Angew. Chem., Int. Ed.*, 2025, **64**, e202504667.
22 H. Li, K. Liu, J. Fu, K. Chen, K. Yang, Y. Lin, B. Yang, Q. Wang, H. Pan, Z. Cai, H. Li, M. Cao, J. Hu, Y. Lu, T. Chan, E. Cortés, A. Fratalocchi and M. Liu, *Nano Energy*, 2021, **82**, 105767.
23 Q. He, Y. Zhou, H. Shou, X. Wang, P. Zhang, W. Xu, S. Qiao, C. Wu, H. Liu, D. Liu, S. Chen, R. Long, Z. Qi, X. Wu and L. Song, *Adv. Mater.*, 2022, **34**, 2110604.
24 L. Wang, X. Lv, H. Wang, J. Ren, Y. Feng, M. Sun and Z. Yuan, *Adv. Energy Mater.*, 2025, **15**, e04036.
25 Y. Fan, J. Zhao, J. Zhou, W. Huang, J. Zhu, C. Kuo, S. Zhang, C. Pao, T. Chan, Y. Zhang, S. Hsu, J. Chen, C. Chen, C. Jin, L. Tjeng, J. Wang, Z. Hu and L. Zhang, *Energy Environ. Sci.*, 2025, **18**, 7527–7540.
26 Z. Tang, Z. Dong, L. Yuan, B. Li and Y. Zhu, *EES Catal.*, 2025, **3**, 943–971.
27 X. Wang, G. Long, B. Liu, Z. Li, W. Gao, P. Zhang, H. Zhang, X. Zhou, R. Duan, W. Hu and C. Li, *Angew. Chem., Int. Ed.*, 2023, **62**, e202301562.
28 W. Yan, Y. Mou, M. Li, K. Ma, Z. Xu, T. Lu, H. Du, C. Wang, H. Sun, L. Chen, Y. Tang, Y. Wang and G. Fu, *Adv. Mater.*, 2025, **37**, 2506936.
29 S. Zhang, L. Qing, J. Zhang, Z. Ma, S. Zhan, L. Zhang and T. Liu, *ChemSusChem*, 2025, **18**, e202501807.
30 Y. Zhang, H. Zheng, K. Zhou, J. Ye, K. Chu, Z. Zhou, L. Zhang and T. Liu, *Adv. Mater.*, 2023, **35**, 2209855.
31 S. Zhang, Y. Song, Y. Liu, J. Zhu, Z. Ma, L. Qing, Z. Wang, L. Zhang, T. Liu and Y. Xie, *Adv. Funct. Mater.*, 2026, **36**, e02874.
32 Y. Song, S. Zhang, Y. Liu, Y. Ding, Z. Ma, Y. Liu, W. Fan and L. Zhang, *Compos. Commun.*, 2025, **55**, 102326.

33 Y. Ding, S. Zhang, Y. Liu, Y. Liu, H. Zheng, L. Qing, Y. Song, Z. Ma, L. Zhang and T. Liu, *Adv. Funct. Mater.*, 2025, **35**, 2422339.
34 S. Zhang, Y. Song, Y. Liu, Z. Ma, S. Zhan, Z. Wang, L. Zhang, T. Liu and Y. Xie, *ACS Nano*, 2025, **19**, 31690–31698.
35 Z. Huang, T. Cheng, A. Shah, G. Zhong, C. Wan, P. Wang, M. Ding, J. Huang, Z. Wan, S. Wang, J. Cai, B. Peng, H. Liu, Y. Huang, W. Goddard and X. Duan, *Nat. Catal.*, 2024, **7**, 678–688.
36 M. Liu, H. Su, X. Liu, X. He, P. Tan, F. Liu and J. Pan, *Nat. Commun.*, 2025, **16**, 2826.
37 Z. Wang, Y. Han, Y. Wang, S. Zang and P. Peng, *Angew. Chem., Int. Ed.*, 2025, **64**, e202416973.
38 J. Zhang, L. Zhang, J. Liu, C. Zhong, Y. Tu, P. Li, L. Du, S. Chen and Z. Cui, *Nat. Commun.*, 2022, **13**, 5497.
39 X. Lin, W. Hu, J. Xu, X. Liu, W. Jiang, X. Ma, D. He, Z. Wang, W. Li, L. Yang, H. Zhou and Y. Wu, *J. Am. Chem. Soc.*, 2024, **146**, 4883–4891.
40 T. Zhu, J. Han, T. Sun, J. Zhao, X. Pi, J. Xu and K. Chen, *ACS Catal.*, 2024, **14**, 1914–1921.
41 S. Zhang, Y. Liu, Y. Ding, H. Wu, L. Qing, J. Zhu, S. Chen, Z. Wang, L. Zhang and T. Liu, *Adv. Mater.*, 2025, **37**, 2418681.
42 J. Chen, C. Chen, M. Qin, B. Li, B. Lin, Q. Mao, H. Yang, B. Liu and Y. Wang, *Nat. Commun.*, 2022, **13**, 5382.
43 L. Ren, K. Zhang, Y. Huang, Y. R. Lu, H. Deng, Y. Ding, C. Chen, B. Huang, W. Hua, L. Fu, X. Zhao, S. Shen, J. Wei and J. Chen, *ACS Catal.*, 2025, **15**, 11022–11033.
44 Z. Ma, S. Zhan, Y. Xie, Y. Liu, Y. Ding, S. Zhang, H. Lin, L. Zhang, T. Liu and Y. Xie, *Adv. Mater.*, 2025, **37**, 2420565.
45 J. Wu, X. Wang, W. Zheng, Y. Sun, Y. Xie, K. Ma, Z. Zhang, Q. Liao, Z. Tian, Z. Kang and Y. Zhang, *J. Am. Chem. Soc.*, 2022, **144**, 19163–19172.
46 L. Zhang, Z. Ma, Z. Wu, Y. Liu, J. Bai, S. Zhang, E. Debroye, W. Fan, H. Lin and T. Liu, *Adv. Funct. Mater.*, 2024, **34**, 2404707.
47 C. Xie, W. Chen, S. Du, D. Yan, Y. Zhang, J. Chen, B. Liu and S. Wang, *Nano Energy*, 2020, **71**, 104653.